JOURNAL OF APPLIED PHYSICS **124**, 123901 (2018)

Effective magnetic susceptibility of suspensions of ferromagnetic particles

Kunlun Bai,[1] Joshua Casara,[2] Aparna Nair-Kanneganti,[1] Aubrey Wahl,[1] Florian Carle,[1] and Eric Brown[1,2,a)]

[1]*Department of Mechanical Engineering and Materials Science, Yale University, New Haven, Connecticut 06511, USA*

[2]*School of Natural Sciences, University of California, Merced, California 95343, USA*

(Received 25 May 2018; accepted 1 September 2018; published online 25 September 2018)

The effective susceptibility χ_{eff} of suspensions of ferromagnetic particles in a liquid was measured using inductance measurements. These measurements were used to test a model that predicts how χ_{eff} varies due to demagnetization, as a function of sample aspect ratio, particle packing fraction, and particle aspect ratio [R. Skomski, G. C. Hadjipanayis, and D. J. Sellmyer, IEEE Trans. Magn. **43**, 2956–2958 (2007)]. For spherical particles or cylindrical particles forcibly aligned with an external magnetic field, the model can be fitted to the measured data with agreement within 13%. This model predicts suspensions of aligned, large-aspect-ratio particles should have the largest χ_{eff}, approaching the particle material susceptibility in the limit of large particle aspect ratio. However, χ_{eff} was found to be no larger than about 4 for cylindrical iron particles of various aspect ratios, close to the value obtained for spheres. This results from the random alignment of non-spherical particles relative to the magnetic field naturally found in suspensions, which increases the demagnetization effect and limits χ_{eff}. The contribution of random particle alignments to the demagnetization effect and χ_{eff} remains to be accounted for in models. *Published by AIP Publishing.*
https://doi.org/10.1063/1.5041750

I. INTRODUCTION

Suspensions of magnetic particles in a liquid can be controlled by an applied magnetic field, a property that is taken advantage of, for example, in the fields of ferrohydrodynamics[2] and magnetorheology.[3] The parameter that directly controls the force applied by a magnetic field in these cases is the effective magnetic susceptibility χ_{eff}. If the suspensions are also conducting, magnetohydrodynamic effects can occur such that a magnetic field can in principle be generated by the conducting fluid flow, and the magnetic field can deflect the conducting flow via a Lorentz force, effects whose magnitude scales with $1+\chi_{eff}$.[4–6] These phenomena are not easily achieved with known fluids—pure conducting liquids generally have a magnetic susceptibility $\chi \ll 1$. On the other hand, there is potential that if a material can be designed with large enough $\chi_{eff} \gtrsim 1$, these phenomena could be more easily observed on a laboratory or device scale of order 10 cm.[7] Our goal is to determine how the effective magnetic susceptibility χ_{eff} depends on the properties of suspensions. In particular, we would like to determine the largest values of χ_{eff} that can be obtained, as larger values would make such suspensions more useful for producing magnetohydrodynamic phenomena on the laboratory scale.

The effective susceptibility χ_{eff} is defined by the proportionality $\chi_{eff} = \phi M/H_{app}$, where H_{app} is an externally applied magnetic field, M is the magnetization per unit volume of magnetic material, and ϕ is the packing fraction by volume of the magnetic particles. Note that the factor of ϕ in the expression differs from traditional definitions in pure materials where the sample is 100% magnetic material—here we define χ_{eff} as susceptibility per unit volume of sample, since we are interested in the force from an applied magnetic field on the sample as a whole. For linear magnetic materials χ_{eff} is independent of H_{app}, in practice, this tends to be the case for small H_{app} before the magnetization begins to saturate.

Locally, the magnetic susceptibility $\chi = M/H$ is considered an infinite bulk material property depending on the local magnetic field H. In contrast, χ_{eff} as a macroscopic parameter can be much smaller than χ due to demagnetization, an effect in which the induced magnetic dipole creates an additional magnetic field DM (where D is called the demagnetization factor) that opposes H_{app}. The net magnetic field inside the material $H_{app} - DM$ that determines the net local magnetization M is less than H_{app}, resulting in χ_{eff} being smaller than χ. While D is not necessarily a uniform scalar quantity except for uniformly magnetized ellipsoids, it is often approximated as such for the purpose of performing tractable calculations. The effective susceptibility can then be written such that the demagnetization is a correction factor on the material susceptibility:

$$\frac{\phi}{\chi_{eff}} = \frac{1}{\chi} + D. \tag{1}$$

It is well-known for single-piece solid magnets, for example, that D depends on the shape of the magnet. In particular, D is small in the limit of long, thin magnets aligned with the applied magnetic field—in this limit, χ_{eff} approaches the material susceptibility χ. For single-piece solids, unless the aspect ratio of the material is extremely large, $\chi_{eff} \ll \chi$ and to a good approximation, $\chi_{eff} \approx \phi/D$. χ_{eff} has been

a)eric.brown@yale.edu

calculated for many particle shapes.[8] For example, for a spherical particle $D = 1/3$, resulting in a maximum $\chi_{eff} \approx 3$ as long as $\chi \gg 3$. For such geometries with aspect ratio close to 1, the demagnetization effect can be considered a dominating factor determining χ_{eff}, rather than a small perturbation on the material susceptibility χ.

Demagnetization factors are less well-understood for systems of random arrangements of particles such as suspensions. With many particles, the demagnetization factor D can depend on geometries of both the particles and the sample as a whole, as well as positions and alignments of particles relative to each other and the applied magnetic field.

For randomly packed spherical particles, it has been theoretically argued that the demagnetization factor is $D = \frac{1}{3}(1 - \phi) + D_g\phi$, where D_g is the global demagnetization factor based on the geometry of the sample.[9] D_g was assumed to have the same value as the demagnetization factor for a single particle of the same shape. A numerical calculation confirmed that this model is a good approximation within 3% for a sample of randomly packed spherical particles for sample aspect ratios $\gamma_g = 0.5$ to 1 and packing fractions ϕ from 0.4 to 0.6.[10] It remains to be seen how well the prediction holds over a wider parameter range, in particular, at larger γ_g where χ_{eff} is expected to be larger.

A more general model takes advantage of the fact that exact expressions can be found for homogeneously magnetized ellipsoids of revolution to obtain an expression for identical ellipsoidal particles homogeneously dispersed in any non-magnetic medium (including suspensions) in which particles are aligned with each other and the external magnetic field.[1] Replacing the factor of $1/3$ for spheres[9] with a more general function D_p which is the demagnetization factor of each particle yields[1]

$$D = D_p(1 - \phi) + D_g\phi. \tag{2}$$

Here D_p may be different from the global demagnetization factor D_g and so is an unknown function of particle geometry. Equation (2) may be interpreted as a weighted average of D_p and D_g in ϕ, where D_p dominates at small ϕ where the demagnetization fields of particles do not interact with each other, and D_g dominates at large ϕ where there is a lot of overlap of magnetic fields of neighboring particles so the overall sample shape mainly determines the magnetic field lines. An expression for χ_{eff} can be obtained by combining Eqs. (1) and (2), which simplifies if demagnetization effects are as significant as they are for typical single-piece ferromagnetic materials in the limit where $\chi \gg \chi_{eff}$ to

$$\chi_{eff} \approx \frac{\phi}{D_p(1 - \phi) + D_g\phi}. \tag{3}$$

Since D_p and D_g are expected to be small for large aspect ratios, this model makes a practically important prediction: that in the limit of large particle aspect ratios γ_p and large sample aspect ratios γ_g, χ_{eff} will approach the material susceptibility χ. To our knowledge, it has not yet been tested whether this model captures the effects of different particle shapes on χ_{eff}, and there is no model or data on how D_p depends on particle aspect ratio or other parameters.

In this manuscript, we test the applicability of Eq. (3) to suspensions of spherical and cylindrical particles by measuring χ_{eff} over a wide range of packing fraction ϕ, sample aspect ratio γ_g, and particle aspect ratio γ_p. The remainder of the manuscript is organized as follows. We first describe the suspensions used in Sec. II A. We describe the gradiometer used to measure χ_{eff} in Secs. II B–II D. We test the linearity of the magnetic response of the suspensions in Sec. III A. Measurements of χ_{eff} as a function of ϕ, γ_g, and γ_p are reported in Sec. III B. We test the model in the case of particles aligned with the magnetic field in Sec. III C. Finally, in Sec. III D, we test whether particle alignment with the magnetic field plays an important role in χ_{eff}, an effect which was not accounted for in Eq. (3).

II. MATERIALS AND METHODS

A. Materials

We suspended iron particles (density 7834 kg/m^3 and purity 99.5%) of mean diameter 29 μm, where 90% of particle diameters are within the range 18–40 μm, purchased from Chemicalstore.com. The particles are nearly spherical with a standard deviation of 4% in the diameter. We use these nearly spherical particles in experiments unless otherwise specified. The suspending liquid was a eutectic alloy of gallium and indium known as eGaIn (density 6250 kg/m^3), which was produced as described in Ref. 7. We used a liquid metal for its potential in magnetohydrodynamic applications. The properties of the liquid metal are not expected to be important here, other than the effect of its conductivity 3.40×10^6 S/m[11] contributing to stronger eddy currents that could reduce χ_{eff} at high frequencies of applied alternating magnetic field (see Sec. III A). Samples were kept in a bath of hydrochloric acid at pH < 0.9 to prevent oxidation of the metals.[7] Dry granular samples were obtained by mixing the iron particles with non-magnetic sand.

In both suspensions and dry granular samples, the packing fraction ϕ was obtained by measuring masses of the constituent materials and using density to convert to a packing fraction by volume of the magnetic material (iron) divided by the total volume taken up by the sample. In the case of dry granular samples, the total volume of the sample was measured as the volume taken up in the sample container, which includes air.

B. Experimental setup

Measurements were taken using a gradiometer which consists of two pairs of inductor coils shown in Fig. 1. The gradiometer measures χ_{eff} of a material sample based on how it changes the mutual inductance between two surrounding coils P_1 and S_1. The sample sits in a cylindrical tube which is placed inside the secondary coil S_1, while coil S_1 is inside the primary coil P_1. There is another nominally identical set of coils P_2 and S_2. An alternating current I_p is applied at frequency f (angular frequency $\omega = 2\pi f$) through the primary coils P_1 and P_2, while the induced voltage ε_{ind} is measured across both the secondary coils S_1 and S_2. The secondary coils are linked in the opposite direction in the circuit

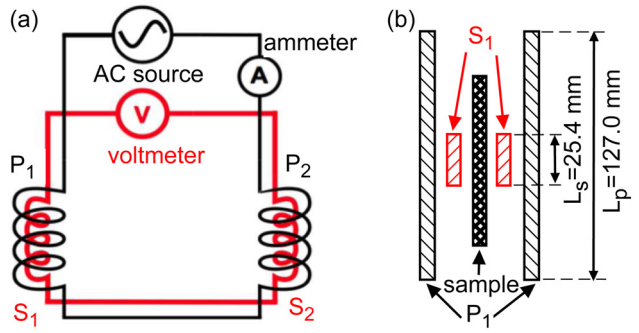

FIG. 1. (a) The circuit diagram of the gradiometer used to measure the effective susceptibility χ_{eff} of a sample based on the change in mutual inductance of a solenoid pair. (b) A diagram (not to scale) that shows a cross section of the coils and sample.

such that the mutual inductances of each pair of primary and secondary coils—M_1 and M_2, respectively—cancel in their contribution to the measured ε_{ind} when there is no sample inside coil S_1.

We intend to measure in the linear material response range so as not to mix demagnetization effects with saturation effects in the measurements. In theory, the induced voltage is then proportional to χ_{eff}. In practice, the two pairs of coils are not identical which we account for with a small correction factor $\Delta M = M_1 - M_2$. Furthermore, there is a background voltage noise ε_{noise} measured when there is no sample and no applied current. In the linear material response range, the theory of induction allows derivation of an expression for the induced voltage ε_{ind}

$$\varepsilon_{ind}^2 = \varepsilon_{noise}^2 + \omega^2 I_p^2 [\alpha M_1 \chi_{eff} + \Delta M]^2, \tag{4}$$

where α is the fraction of volume of coil S_1 filled by the sample. This expression assumes that the background noise is distributed among all phases, which differs from the fixed phase of the induction signal so that the root-mean-square values of their respective contributions to the induced voltage are added in quadrature.

The geometric parameters of the system are as follows. The primary coil P_1 has length $L_p = 127.0 \pm 0.2$ mm, diameter $d_p = 50.8 \pm 0.2$ mm, and $N_p = 332 \pm 22$ turns of wire. The secondary coil S_1 has length $L_s = 25.4 \pm 0.2$ mm, diameter $d_s = 14.8 \pm 0.2$ mm, and $N_s = 190 \pm 14$ turns of wire. The coils S_2 and P_2 are nominally identical to S_1 and P_1, respectively. All suspensions were prepared in cylindrical containers of length L that satisfies $L_s < L < L_p$ to minimize fringe effects. The filling fraction of the coil S_1 is then given by $\alpha = d^2/d_s^2$, where d is the diameter of the sample. We aligned the sample vertically within coil S_1 by finding the position of maximum measured induced voltage, as misalignment along the axis of the cylinder results in a reduced signal. The samples had inner diameter $d = 10.2 \pm 0.1$ mm unless otherwise specified, corresponding to a typical filling factor $\alpha = d^2/d_s^2 = 0.471$. The sample aspect ratio is given by $\gamma_g = L/d$.

Here we summarize some typical electrical measurement parameter values and errors. All electrical components, including those outside the coils, remained in an identical configuration from run to run to minimize errors. We report root-mean-square values for all of our measurements of both alternating current and voltage throughout the paper. For our measurements, the applied alternating current is typically $I_p = 65 \pm 0.5$ mA (corresponding to an 0.8% error) unless otherwise noted, and the uncertainty in the measured ε_{ind} is $0.06\%\varepsilon_{ind} + 0.04$ mV, as given by the manufacturer (Agilent model 34401A multimeter). We typically report measurements at frequencies f ranging from 200 to 2000 Hz, and χ_{eff} is calculated from Eq. (4), using an unweighted average over this frequency range unless otherwise specified. At these typical measurement values, and, for example, when $\chi_{eff} \geq 1.3$ (corresponding to $\phi \geq 0.18$), we measure $\varepsilon_{ind} \geq 10$ mV, with a voltage uncertainty $\leq 0.4\%$, which is generally less than the uncertainty on the current measurement. The noise term ε_{noise} is due to electronic noise, and as such, varies when the measurement equipment is on. It is thus measured as ε_{ind} at a weak signal with frequency $f = 5$ Hz at $I_p = 65$ mA. We measured $\varepsilon_{noise} = 3$ mV on average, with a standard deviation of 0.4 mV over the course of a series of experiments shown in one plot, or 1 mV over the longer time scale of different measurement series. When added in quadrature as in Eq. (4), this leads to an error on ε_{ind} of less than 0.5% for $\chi_{eff} \geq 1.3$, for example, which is small compared to the other errors for these typical measurement parameters. This error becomes dominant when the signal is smaller, notably where we test the linearity of the signal at small values of I_p or f in Sec. III A, or small ϕ where $\chi_{eff} \ll 1$. Similarly, the absolute error on χ_{eff} from the error of ΔM is 0.01, or equivalently less than 0.8% of $\alpha M_1 \chi_{eff}$ when $\chi_{eff} \geq 1.2$ for the typical measurement parameters (see Sec. II C on how values of M_1 and ΔM are obtained). Thus, the largest systematic source of error in calculating χ_{eff} from Eq. (4), unless otherwise noted, typically comes from the 0.8% on the applied current I_p for our typical parameters and $\chi_{eff} \geq 1.2$.

When we repeated measurements by turning off the electronics, taking a sample container out from inside the coils, putting the sample back, and turning on the electronics again, the run-to-run standard deviation was 2.5% for suspensions and granular samples and 0.2% for macroscopic solid pieces. The larger run-to-run variation of suspensions and powders may come from the rearrangement of particles as the sample containers are disturbed, but it is smaller than the 6% standard deviation observed in numerical simulations.[10]

C. Inductance calibration

To provide calibration values of M_1 and ΔM in Eq. (4), we measure the mutual inductances of each coil independently without a sample, in each case removing the other coil from the circuit and measuring without a sample. In these cases, the measured voltage is expected to be

$$\varepsilon_{ind}^2 = \varepsilon_{noise}^2 + \omega^2 I_p^2 M_i^2, \tag{5}$$

where $i = 1$ or 2 is the coil pair index number. Measurements of ε_{ind}^2 are shown as a function of $\omega^2 I_p^2$ in Fig. 2 for both coil pairs. We fit Eq. (5) with ε_{noise} and M_i as fit parameters for each pair to obtain the slopes M_1 and M_2,

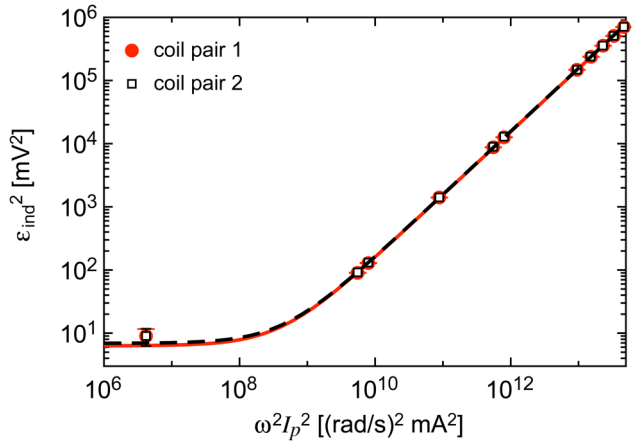

FIG. 2. Induced voltage from the mutual inductance of each pair of solenoid coils in isolation. Solid circles: coils P_1 and S_1. Open squares: coils P_2 and S_2. The slopes of the fits yield the squares of the mutual inductances M_1 (solid line) and M_2 (dashed line), and the constant at low-frequency yields the square of ε_{noise}. These parameters are used for calibration of the apparatus.

respectively. The error bars in the figure represent the sum of a 0.2% standard deviation of multiple repetitions and a 0.8% systematic error, except for the lowest frequency point which is the one used to obtain the value of ε_{noise} where the uncertainty on the voltage measurement was much larger. To obtain a fit with a reduced Chi-squared of 1 (where the reduced Chi-squared value of a fit corresponds to the mean-square difference between the data and fit, normalized by the error), we increase the percentage input errors to 1.6% and 1.9% for the higher-frequency points of coil pairs 1 and 2, respectively. The fit yields $M_1 = (1.245 \pm 0.004) \times 10^{-4}$ H and $M_2 = (1.253 \pm 0.004) \times 10^{-4}$ H. These measured values are consistent with the expected theoretical value $M = N_p N_s A_s / L_p = (1.2 \pm 0.1) \times 10^{-4}$ H based on the dimensions of the setup, where $A_s = \pi d_s^2/4$ is the cross-sectional area of the secondary coil. The difference between these measured mutual inductances is $\Delta M = M_2 - M_1 = (8 \pm 6) \times 10^{-7}$ H. These values M_1 and ΔM are used as calibrations to calculate χ_{eff} from Eq. (4). The lowest-frequency point in Fig. 2 is seen to be well above an extrapolation of the linear scaling found at high frequency, confirming that this frequency is low enough to measure ε_{noise}.

D. Susceptibility calibration

We used single-piece solid cylindrical samples to calibrate χ_{eff} measurements in our setup. To account for the demagnetization effect, we use for reference a numerical simulation of the demagnetization factor D for single-piece cylindrical samples of various aspect ratios γ from Chen *et al.*,[12,13] shown in Fig. 3. We fit the function

$$D = A\gamma^n \tag{6}$$

to this data, over the range $2 < \gamma < 50$, which covers our measurement range. We adjusted the input error to be 11% to obtain a reduced Chi-squared of 1, yielding $A = 0.40 \pm 0.04$ and $n = -1.35 \pm 0.04$.

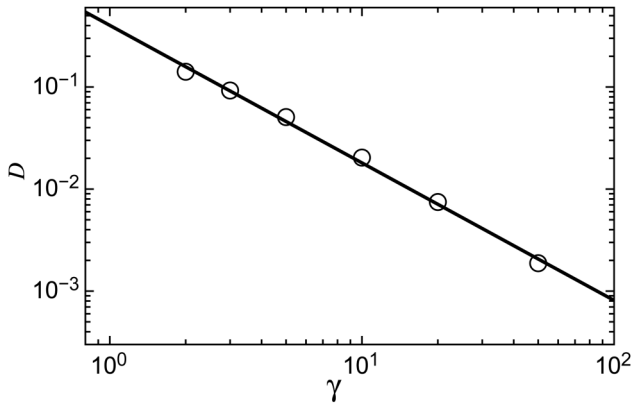

FIG. 3. Demagnetization factor D for a single-piece cylindrical sample as a function of aspect ratio. The data are reproduced from Chen *et al.*[12] A power law is fit to obtain a reference curve to account for the demagnetization effect in single-piece solids.

To calibrate our setup, we measured χ_{eff} of single-piece solid samples for different aspect ratios in Fig. 4. We used different grades of ferrite from National Magnetics Group, and iron from Fair-rite. The values of material susceptibility χ given by the suppliers and diameters d with uncertainties of up to 0.3 mm are given in the legend of Fig. 4. A reference curve χ_{ref} is shown in Fig. 4 for each material, which is calculated by inserting the fit function for D [Eq. (6)] into Eq. (1) with $\phi = 1$. Since $\chi \gg 1$ for all of these materials, the predicted χ_{ref} curves are all close to each other. While the data tend to follow similar trends as the expected calibration curves, there are significant differences.

To come up with an appropriate calibration adjustment, we first consider that sample aspect ratio may not be the primary parameter which it could depend on. In the ideal theory assumed in Eq. (4), if $L_s \ll L \ll L_p$, the magnetic field inside S_1 is expected to be uniform. In practice, fringe effects may add a correction. To come up with a calibration

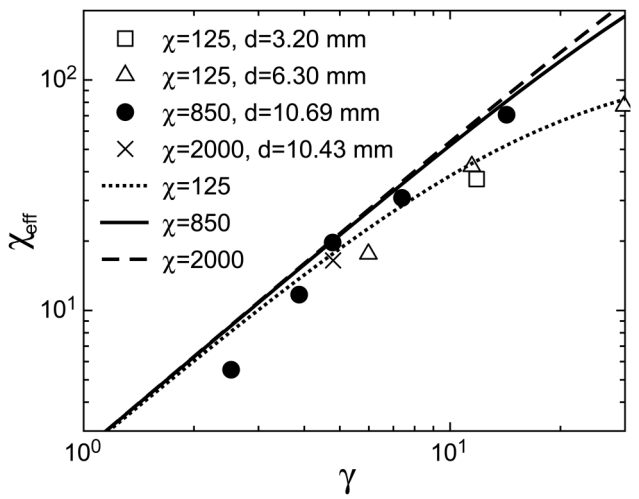

FIG. 4. Measured effective susceptibility χ_{eff} of single-piece solid samples as a function of aspect ratio γ. Data are shown for different material susceptibility χ and diameters d as indicated in the legend. Lines: reference curves based on the simulation results of Chen *et al.*,[12] for the different material susceptibilities χ given in the legend.

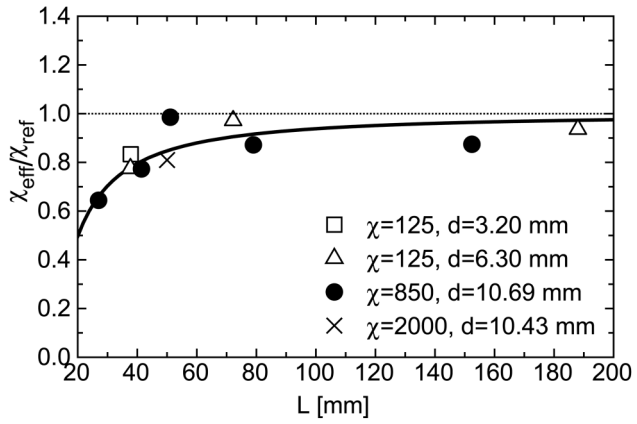

FIG. 5. Ratio between the measured effective susceptibility χ_{eff} for single-piece solid samples and the reference value from Chen *et al.*,[12] as a function of sample length L. Data are shown for different material susceptibility χ and diameters d as indicated in the legend. Solid line: fit of data to obtain a calibration function for correcting later data.

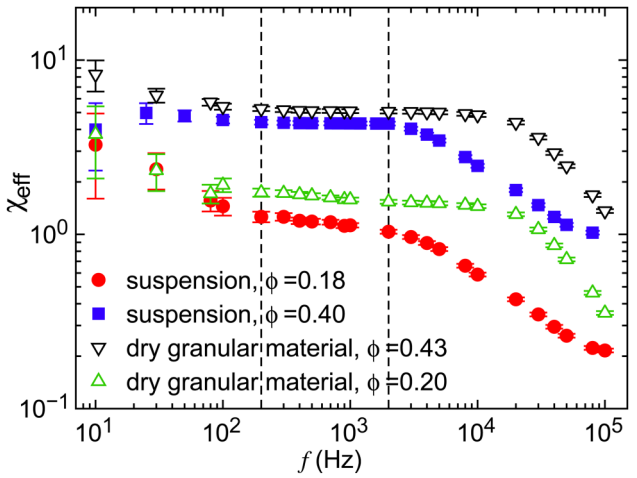

FIG. 6. Examples of χ_{eff} as a function of frequency f. Solid symbols: suspensions of iron particles in eGaIn at $\phi = 0.18$ (circles) and $\phi = 0.40$ (squares). Open symbols: dry granular materials at $\phi = 20\%$ (up-pointing triangles) and $\phi = 43\%$ (down-pointing triangles). χ_{eff} reaches a plateau for $f < 2000$ Hz. The vertical lines indicate the bounds of the frequency range where χ_{eff} is averaged over for measurements reported in other plots.

adjustment as a function of the sample length L, we replot our measurements of χ_{eff} for single-piece samples from Fig. 4 normalized by the reference curve χ_{ref} as a function of the sample length L in Fig. 5. A systematic dependence on L is observed in Fig. 5, similar to the trend in Fig. 4. In contrast, there is no significant systematic trend in d. This confirms the calibration should be made as a function of L, but not as a function of d. We fit the data to a power law to obtain calibration function $\chi_{eff}/\chi_{ref} = 1 - 25.8L^{-1.30}$ when L is in units of mm. This calibration function fits the data with a root-mean square difference of 7.6%. Our data presented in Secs. III B–III D, where quantitative values are of interest, is divided by this calibration function. Based on the variation of the fit around the data, we introduce an error of 7.6% from fringe effects and other unknown sources when comparing samples in all following measurements of χ_{eff}. For much of our data, where we have a constant $L = 112$ mm, this amounts to an upward correction of 5% on the data and does not affect trends.

III. RESULTS

A. Linearity of magnetic response

To characterize the magnetic susceptibility of suspensions as a function of sample aspect ratio, particle packing fraction, and particle aspect ratio, we first check whether we can characterize each sample by a well-defined χ_{eff}, i.e., a value that is independent of the frequency f and magnitude H_{app} of the applied magnetic field. To test the frequency-dependence, some examples of the measured susceptibility χ_{eff} are shown for dry granular materials and suspensions as a function of frequency f in Fig. 6, at sample aspect ratio $\gamma_g = 11$, length $L = 112.2$ mm, and packing fractions ϕ shown in the legend. The error bars plotted are the quadratic sum of the 2.5% run-to-run standard deviation and the 0.4 mV error on the noise voltage measurements. The 0.4 mV error leads to a large error at low frequencies where the signal is weak. A plateau in χ_{eff} is found at frequencies $f < 2000$ Hz for all suspensions of nearly spherical particles reported in this paper. At higher frequencies, χ_{eff} decreases, qualitatively similar to the frequency response of other magnetic materials. The decrease in χ_{off} starts at lower frequencies for suspensions than dry granular materials, which may be expected due to stronger eddy currents in the higher conductivity suspensions which oppose the applied magnetic field more strongly at higher frequency.

To identify a characteristic χ_{eff} for each sample, we use the value of χ_{eff} in the low-frequency plateau. This plateau is typical of ferromagnetic materials, and so it is expected that this plateau value is the relevant value of χ_{eff} down to the DC limit at low frequencies. At frequencies $f < 200$ Hz, the data remain consistent with the plateau, however, there are large relative uncertainties in this range due to the low voltage signal. Thus, in other plots in this paper, we report the averaged χ_{eff} over the range of 200 Hz to 2000 Hz as the representative value for the low-frequency plateau, unless we specify otherwise that we found the low-frequency plateau in a different range. This could introduce an error if there is a trend in χ_{eff} with frequency, as seen for $\phi = 18\%$ suspension in Fig. 6. In this case, which is comparable to the worst case, using the mean of χ_{eff} for frequencies in the range of 200 Hz to 2000 Hz can underestimate a fit in the zero-frequency limit by up to 3%.

We next test whether the magnetic response is linear in the applied magnetic field H_{app} (equivalently, whether χ_{eff} is independent of H_{app}) and whether the suspensions behave more like paramagnetic or ferromagnetic materials. We plot the magnetization per unit volume of sample $\phi M = \chi_{eff} H_{app}$ vs. the applied magnetic field $H_{app} = I_p N_p / L_p$ in Fig. 7 for a suspension with $\phi = 0.34$, $\gamma_g = 2.5$, and $L = 25.40$ mm. We show these measurements with histories of both increasing and decreasing applied current I_p ($\propto H_{app}$). It is seen in Fig. 7 that these ramps give equivalent results, indicating a lack of hysteresis in the measured range. To test the linear response, we fit a linear function with a constant offset to these data where the random error is the quadratic sum of the 2.5% run-to-run standard deviation and the 0.4 mV random

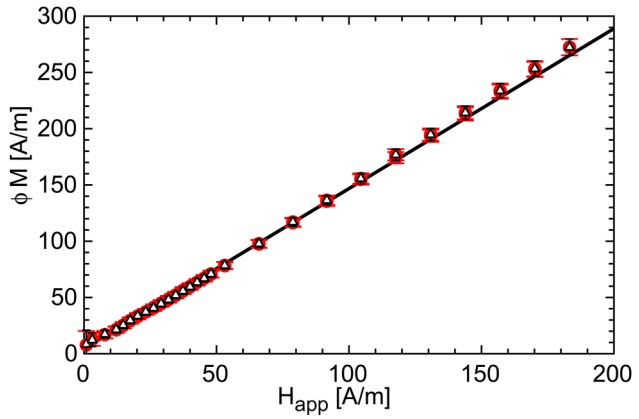

FIG. 7. Magnetization per unit volume of sample $\phi M = \chi_{eff} H_{app}$ of suspensions as a function of applied magnetic field H_{app}. Closed circles: increasing H_{app} (or I_p). Open triangles: decreasing H_{app} (or I_p). Line: linear fit. The suspension behaves as a linear paramagnetic material, with no hysteresis or significant remnant magnetization.

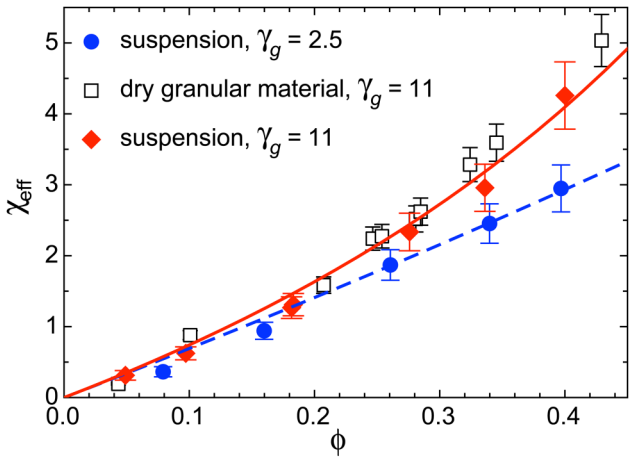

FIG. 8. Effective susceptibility χ_{eff} as a function of packing fraction ϕ for spherical particles ($\gamma_p = 1$). Solid symbols: suspensions at sample aspect ratio $\gamma_g = 11$ (diamonds) and $\gamma_g = 2.5$ (circles). Open squares: dry granular material at $\gamma_g = 11$. The suspensions exhibit a slightly smaller χ_{eff} than dry granular materials at the same sample aspect ratio $\gamma_g = 11$. Lines: fit of Eq. (7) for suspensions at $\gamma_g = 11$ (solid line) and $\gamma_g = 2.5$ (dashed line), where fit parameters are obtained from simultaneously fitting data of Figs. 8–10.

error on voltage measurements, which yields a reduced Chi-squared of 0.8. The consistency of the linear fit with the data confirms the data are consistent with a χ_{eff} independent of H_{app} over this range, verifying the linearity assumed in deriving Eq. (5). The error bars plotted in Fig. 7 include both these systematic and random errors. The constant offset in the linear fit is 5 A/m, which is consistent with $M = 0$ at $H = 0$ within the error of 12 A/m on M at that point due mainly to the 0.5 mA systematic error on the current. Since we find M consistent with zero at $H_{app} = 0$ with a history of decreasing H_{app}, then there is no resolvable remnant magnetization. The lack of hysteresis or remnant magnetization indicate that the suspensions behave as linear paramagnetic materials in this range, despite the fact that the particles consist of a ferromagnetic material. This is likely because the particles are able to move around in the liquid and reorient more freely than molecular dipoles in magnetic domains in a solid.

B. Variation of χ_{eff} with aspect ratios and packing fraction

Now that we have calibrated the apparatus and established linearity of the response over our measurement range, we now measure the dependence of the effective susceptibility χ_{eff} on the sample packing fraction ϕ, sample aspect ratio γ_g, and particle aspect ratio γ_p to test and fit the model predictions of Eq. (3).

Figure 8 shows how χ_{eff} varies with packing fraction ϕ for two series of suspensions and one of dry granular materials with spherical particles ($\gamma_p = 1$), and sample aspect ratios $\gamma_g = 2.5$ and 11. Plotted errors in this section correspond to the quadratic sum of the systematic and random errors: 1 mV on the voltage, 0.8% on the current, 3% uncertainty on measuring χ_{eff} over a frequency range (Fig. 6), 2.5% run-to-run deviation, and 7.6% uncertainty based on the calibration in Fig. 5. Measurements are shown in Fig. 8 for packing fractions up to the liquid-solid transition $\phi_c = 0.407 \pm 0.003$ for the suspension, defined as the lowest packing fraction where a non-zero yield stress is measured. Measurements of the yield stress for these samples were reported in a previous paper.[7] For each series, χ_{eff} increases with increasing ϕ. On average, χ_{eff} of dry granular materials is higher than that of these suspensions by 11% at the same ϕ.

Figure 9 shows the effective susceptibility χ_{eff} as a function of sample aspect ratio γ_g, for spherical particles ($\gamma_p = 1$) and $\phi = 0.4$. To vary γ_g and satisfy the condition $L_s < L < L_p$, the sample diameter d had to be varied along with the length. We use $d = 10.2 \pm 0.1$ mm for $\gamma_g < 15$, $d = 7.1 \pm 0.1$ mm for $\gamma_g = 19$, and $d = 3.7 \pm 0.1$ mm for $\gamma_g > 22$. At small γ_g, χ_{eff} increases with γ_g and reaches a plateau for $\gamma_g \gtrsim 10$.

To test the dependence of χ_{eff} on particle aspect ratio γ_p in Eq. (3) which assumes that particles are aligned with the applied magnetic field, we made dry samples of stacked

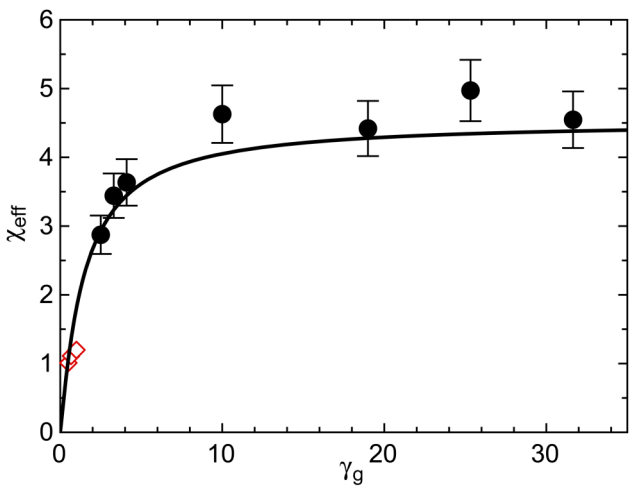

FIG. 9. Effective susceptibility χ_{eff} of suspensions as a function of sample aspect ratio γ_g. Solid symbols: spherical particles ($\gamma_p = 1$) at $\phi = 0.40$. Line: model result of Eq. (7), where fit parameters are obtained from simultaneously fitting data of Figs. 8–10. Open Symbols: numerical simulation of spherical particles at $\phi = 0.40$.[10]

cylindrical particles where the particles were forced to be aligned with the applied magnetic field. To make such aligned samples while holding γ_g and ϕ constant, we cut a 130 mm long cylindrical ferrite rod into collections of gradually smaller pieces to obtain a series of decreasing γ_p. Each piece was nearly cylindrical, with roughness on a scale of 1 mm at the two ends of the cylinder due to the cutting process. The packing fraction ϕ ranged from 100% to 97% due to some loss of material. This resulted in a number of pieces ranging from 1 for the largest γ_p to 32 for the smallest γ_p of the series. The pieces were arranged in a stack in the sample container with a common cylindrical axis aligned with the applied magnetic field. The measured χ_{eff} as a function of γ_p for these aligned particles is shown in Fig. 10 for two series, one with $\gamma_g = 20$ and one with $\gamma_g = 11$. χ_{eff} initially increases with increasing γ_p and levels off for larger γ_p.

C. Testing the model for χ_{eff}

The measurements of χ_{eff} presented in Sec. III B over a wide range of packing fraction ϕ, sample aspect ratio γ_g, and particle aspect ratio γ_p now allow us to test the model of Eq. (3). In Eq. (3), the demagnetization factors D_g and D_p are functions of sample and particle geometry, respectively. To fit parameters, we assume that both D_g and D_p follow power laws of the form $D = A\gamma^n$ as shown in Fig. 3 for single-piece solid magnets.[12] Inserting this form into Eq. (3) with different fit parameters for D_g and D_p yields our fit function

$$\chi_{eff} = \frac{\phi}{A_p\gamma_p^{n_p}(1-\phi) + A_g\gamma_g^{n_g}\phi}. \tag{7}$$

We simultaneously least-squares fit all our suspension data shown in Figs. 8 and 9 and the dry aligned cylinder data in Fig. 10 to Eq. (7) to obtain the fit parameters A_g, n_g, A_p, and n_p. Input errors correspond to the same errors plotted in Sec. III B. Plots of Eq. (3) with these fit parameters are shown in Figs. 8–10, where it is seen that the model captures the trends of χ_{eff} in ϕ, γ_g, and γ_p, respectively. Using the input errors on the data from Sec. III B results in a reduced Chi-squared of 1.1, indicating that the model function is as good as can be obtained with our uncertainty. The root-mean-square difference between the data and the model is 13%, corresponding to the uncertainty, we can put on the model predictions using fit parameters from our data. This 13% variation is close to the 11% systematic difference between the dry granular samples and suspensions in Fig. 8. This and the fact that the model was also fit to the dry particles data in Fig. 10 indicates that both dry granular materials and suspensions can be self-consistently described by the same function within this 13% error. The best fit parameters for Eq. (7) are $A_g = 0.33 \pm 0.07$, $n_g = -1.11 \pm 0.08$, $A_p = 0.147 \pm 0.005$, and $n_p = -4.4 \pm 0.2$. The best fit values of A_g and n_g are consistent with the fit values $A = 0.31 \pm 0.01$ and $n = -1.12 \pm 0.02$ from the single-piece cylinder data of Chen *et al.*[12] in Fig. 3, confirming that D_g in Eq. (3) is consistent with the demagnetization factor D of individual cylindrical particles.[10] This agreement of values for different particle shapes (e.g., spheres and cylinders) suggests the values we found for A_p and n_p also apply to particles of different shapes aligned with the applied magnetic field within the 13% error.

To compare to previous work in Fig. 9, we show numerical simulation results of randomly packed spherical particles at $\phi = 0.4$.[10,14] The simulation data are in reasonable agreement with the model.

An alternate model by Martin *et al.* for χ_{eff} was proposed that does not account for the demagnetization effect, but is designed for the limit of high packing fraction ϕ.[15] It assumes that magnetic field lines tend to go from one ferromagnetic particle to another along regions of high susceptibility, and thus concentrate their density in paths along the shortest distances between particles. It predicts that χ_{eff} diverges at a packing fraction ϕ_c where the gaps between neighboring magnetic particles go to zero according to

$$\chi_{eff} \approx \frac{1}{1-(\phi/\phi_c)^{1/3}} - 1, \tag{8}$$

until it approaches the material susceptibility χ.[15] The value of $\phi_c = 0.74$ suggested by Martin *et al.*[15] is unrealistically large for the packing fraction where the nearest-neighbor particles in a randomly arranged suspension just barely touch each other.[16] A more realistic value for ϕ_c corresponds to the jamming transition, which has a much smaller value for random arrangements of particles than for crystalline packings.[17–19] Our suspensions of spherical particles have a jamming transition at $\phi_c = 0.407$, measured as the lowest packing fraction where the samples exhibit a non-zero yield stress like a solid.[7] We observe in Fig. 8 that χ_{eff} does not diverge to reach the material susceptibility at $\phi_c = 0.407$. This is consistent with the observations of Martin *et al.*,[15] who also did not observe any evidence of a divergence. Furthermore, Fig. 10 shows $\chi_{eff} < 100 \ll \chi$ even in the limit of $\phi \approx 1$, indicating that the divergence to the material susceptibility χ does not exist for any value of packing fraction.

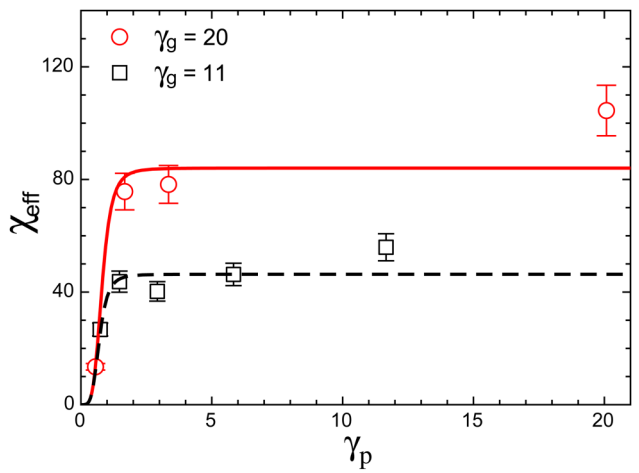

FIG. 10. Effective susceptibility χ_{eff} of packings of cylindrical rods forced to be aligned with the applied magnetic field as a function of particle aspect ratio γ_p, with $\phi \approx 100\%$. Values of γ_g are given in the legend. Lines: model result of Eq. (7) for $\gamma_g = 11$ (dashed line) and $\gamma_g = 20$ (solid line), where fit parameters are obtained from simultaneously fitting data of Figs. 8–10. The simultaneous fits here and in Figs. 8 and 9 confirm the validity of Eq. (7) within a root-mean-square difference of 13%.

This model of Martin *et al.*[15] also fails to explain the dependence of χ_{eff} on sample aspect ratio γ_g shown in Figs. 8 and 9. That model treats χ_{eff} as a bulk property that does not depend on sample shape or size. The dependence of χ_{eff} on γ_g rules out the possibility of χ_{eff} being a bulk property. On the other hand, this leveling off of χ_{eff} at a value much lower than the bulk susceptibility χ conforms with expectations of the demagnetization effect, similar to single-piece solid magnets. According to the model of Skomski *et al.*,[1] χ_{eff} is limited both by the order of the sample aspect ratio γ_g and particle aspect ratio γ_p. This limitation from the demagnetization effect also explains why the divergence of χ_{eff} in ϕ predicted by the model of Martin *et al.*[15] cannot be achieved for small aspect ratio particles. These agreements of the data in Figs. 8–10 with Eq. (3) and disagreement with the model of Martin *et al.*[15] confirms the importance of the demagnetization effect in suspensions. As a result, the model of Skomski *et al.*[1] expressed in Eq. (3) with the fit coefficients obtained here more accurately describes $\chi_{eff}(\phi, \gamma_g)$ for suspensions of spherical particles than the model of Martin *et al.*[15]

D. Effect of particle misalignment

In Sec. III C, we tested the model of Eq. (3) for particles aligned with the applied magnetic field, which was an assumption of the model of Skomski *et al.*[1] However, this is not a very practical case for suspensions of aspherical particles, as they tend to have randomly arranged and oriented particles. To characterize how particle misalignment affects χ_{eff}, we made suspensions of cylindrical particles. We purchased iron wire (Goodfellow) and cut it to make cylindrical particles with different particle aspect ratios γ_p. To obtain samples with enough particles to avoid significant finite size effects, while minimizing the number of cuts we needed to make, we used different wire diameters of 0.25, 0.5, and 1 mm for samples with mean particle aspect ratio $\gamma_p > 10$, $5 \le \gamma_p < 10$, and $\gamma_p < 5$, respectively. For samples of aspect ratio $\gamma_g = 4.1$ and length $L = 42$ mm, this results in the ratio of sample diameter to cylinder diameter between 17 and 9, and the ratio of sample diameter to mean particle length between 4.1 and 2.5. This is a parameter range where the value of the packing fraction ϕ_c of the liquid-solid transition is within 4% of the infinite-size system limit.[20,21] Effects of confinement on alignment are also presumed to be small in this system-size range. For example, in this range, the partial particle alignment from this confinement changes the bulk rheology by less than 3%,[21] but to our knowledge, the effect on χ_{eff} from this confinement has not been characterized.

Since sample preparation procedures can affect the alignment of particles, we also characterize the tendency for the particles to align based on different shaking procedures after the sample was loaded into the cell, but before the magnetic field was applied. We used a suspension with sample aspect ratio $\gamma_g = 4.1$, sample length $L = 42$ mm, and particle aspect ratio $\gamma_p = 5.3$, at a packing fraction $\phi/\phi_c = 1.02$. This packing fraction is just barely resolvable to be above the liquid-solid transition, so we can observe the alignment of the particles as they poke out the liquid-air interface. In one case, samples were shaken along the axis of the cylindrical tube to partly align the particles with the external magnetic field, shown in Fig. 11(b). In a second case, the same samples were shaken with a combination of linear and rotational shaking (Vortex Genie 2), resulting in a more random alignment, shown in Fig. 11(c) for the same sample parameters. Note the alignment in the bulk could be quantitatively different from a value based on the particles at the boundary, so these pictures at the surface of the sample should be taken as a coarse characterization of the alignment of particles. These images were analyzed to measure the angle β of each particle relative to the applied magnetic field, which was aligned with the cylindrical tube axis. Figure 11(a) shows the probability distribution $P(\beta)$ for both of these samples. For samples shaken by the vortex mixer, we observe a relatively flat distribution, with a mean angle $\langle\beta\rangle = 44.7°$ corresponding to a random alignment. Samples shaken along the axis direction, while still fairly random, display a preferred alignment angle $\beta = 20°$ and a mean $\langle\beta\rangle = 27.3°$, corresponding to better alignment with the applied magnetic field at $\beta = 0°$.

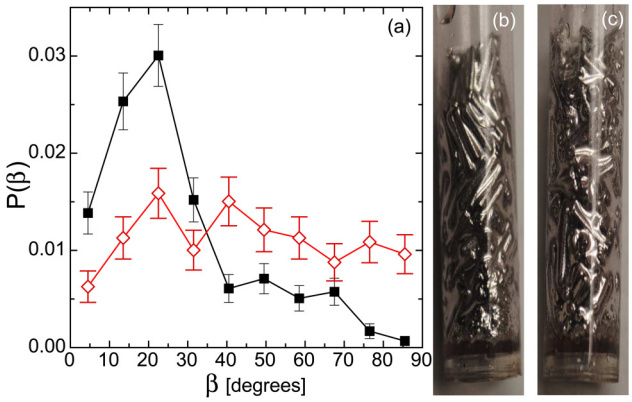

FIG. 11. (a) Probability distribution of particle alignment angles β relative to the applied magnetic field, for samples with length $L = 42$ mm, sample aspect ratio $\gamma_g = 4.1$, particle aspect ratio $\gamma_p = 5.3$, and packing fraction $\phi/\phi_c = 1.02$. Solid squares: samples were shaken along the axis of the cylindrical tube to partly align the particles with the external magnetic field. Open diamonds: samples were shaken using a vortex mixer, resulting in a more random alignment. Pictures of the samples for the 2 shaking procedures are shown in panels (b) and (c), respectively, where the applied magnetic field is aligned in the vertical direction.

Now, we systematically test trends in effective susceptibility χ_{eff} as a function of particle aspect ratio γ_p for suspensions of randomly arranged particles. The measured χ_{eff} is shown as a function of γ_p in Fig. 12, at a fixed relative packing fraction $\phi/\phi_c = 1.02$ (where ϕ_c is the packing fraction of the liquid-solid transition), $\gamma_g = 4.1$, $L = 42$ mm, and for both shaking procedures. The error bars on γ_p indicate the standard deviation of the aspect ratio due to the distribution of particle lengths in each sample. The reason for comparing different shapes at a fixed ratio of ϕ/ϕ_c is that different shapes have different values of ϕ_c[20,21] (values of ϕ_c for each aspect ratio are reported in the Appendix) and the range of packing fractions in the liquid range varies up to ϕ_c. A fixed relative packing fraction $\phi/\phi_c \approx 1$ is near the maximum χ_{eff} expected in the liquid phase for each γ_p, as seen in Fig. 8. Any smaller value of χ_{eff} could be obtained with the same particles at a lower packing fraction.

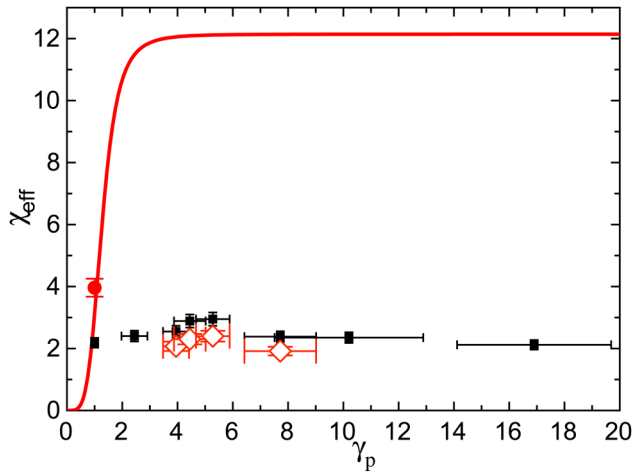

FIG. 12. Effective susceptibility χ_{eff} of suspensions with randomly aligned particles as a function of particle aspect ratio γ_p, at $\gamma_g = 4.1$ and $\phi/\phi_c = 1.02$. Solid squares: samples were shaken beforehand along the axis of the tube to partly align the particles with the external magnetic field. Open diamonds: samples were shaken beforehand using a vortex mixer, resulting in a more random alignment. Solid circle: random packing of spheres ($\gamma_p = 1$), which cannot align or misalign. Solid line: model of Eq. (7). The model overestimates χ_{eff} by about a factor of 4 for suspensions that are misaligned with the external magnetic field.

To test how the model developed for particles aligned with the applied magnetic field applies to randomly arranged particles, the model prediction of Eq. (7) is shown for comparison in Fig. 12. We use the fit parameter values obtained from the simultaneous fit of data in Figs. 8–10 and the power law fit expression for ϕ_c from the fit in Fig. 14 in place of ϕ in Eq. (7). The model overestimates χ_{eff} by about a factor of 4, in this case, where the particles are not aligned with the applied magnetic field. Since that model fit well to data for aligned particles, this indicates the random alignment severely reduces χ_{eff}. χ_{eff} is comparable to the value for spheres, which suggests the demagnetization effect may be about as significant for randomly arranged long cylinders as it is for spheres. It seems likely that the random orientations result in different effective demagnetization factors for different particles that average out to a value of D_p close to that for spheres. The much larger χ_{eff} obtained in Fig. 10 for large γ_p is apparently possible only because the strict alignment of the particles with the applied magnetic field reduces the demagnetization effect.

The trend of higher χ_{eff} with better aligned particles is also seen in our samples with different shaking procedures: the better aligned particles that were shaken along the cylinder axis had a consistently 20% higher χ_{eff} than the more randomly arranged particles that were shaken by the vortex mixer. A simple quantitative estimate of the average vector component of alignment $\cos\langle\beta\rangle$ is also 20% higher for the particles shaken along the cylinder axis then those shaken by the vortex mixer. It suggests, at least in the ballpark, the decrease of χ_{eff} in Fig. 12 may be associated with the change in particle alignment for these two samples of randomly arranged particles. However, extrapolating this simple estimate does not reach the model of Eq. (7). This suggests that much better alignment would be needed to reach that regime than is likely to be obtained in suspensions with even partially randomly arranged particles.

While there is little trend in χ_{eff} over the range of γ_p measured in Fig. 12, it is notable that χ_{eff} exhibits a local maximum in γ_p. In contrast, Eq. (7) predicts χ_{eff} to be a monotonically increasing function of γ_p (as seen in Fig. 10). This local decrease in χ_{eff} with γ_p is not due to the different wire diameters used, as in the range $5 \leq \gamma_p < 10$ where χ_{eff} decreased, the same diameter wires were used. Similarly, finite-size effects cannot explain the peak, as the number of particles is decreasing over the same range of γ_p, which would only be expected to produce more alignment and a larger χ_{eff}, in contradiction to the trend observed in χ_{eff}. It could also be proposed that the local peak in $\chi_{eff}(\gamma_p)$ could be due to a competition between the increasing χ_{eff} in Eq. (7) and the decreasing ϕ_c with γ_p. However, as shown in Fig. 12, the model of Eq. (7) still has no local maximum in this parameter range—even when accounting for this decreasing ϕ_c with γ_p. This insensitivity to ϕ in the model is apparent in the limit of large γ_p of Eq. (3), which becomes $\chi_{eff} \approx 1/D_g$, independent of ϕ. The cause of this local maximum in $\chi_{eff}(\gamma_p)$ remains unknown.

The data in Fig. 12 were taken at $\phi/\phi_c = 1.02$, corresponding to a jammed state where particles were not free to realign in the applied magnetic field. If instead particles were at a lower packing fraction in a liquid state, they might be expected to be able to more freely and better align with the applied magnetic field to reach the higher χ_{eff} predicted by Skomski *et al.*[1] To test this hypothesis, we measured χ_{eff} as a function of packing fraction ϕ for cylinders. We used 0.5 mm diameter wire cut to length 3.2 mm with a standard deviation of 0.6 mm to obtain a particle aspect ratio $\gamma_p = 6.3 \pm 1.3$, near the peak found in Fig. 12. We started with a sample aspect ratio of $\gamma_g = 4.1 \pm 0.3$ at $\phi = 0.42$ in a 10.2 mm diameter tube and diluted the sample with more liquid to increase ϕ. The sample aspect ratio decreased to 3.8 as the liquid-solid transition was crossed and the suspension packed more efficiently, without trapped air. Upon further dilution, the sample aspect ratio increased in inverse proportion to the packing fraction due to the increase in liquid volume. Because the signal was weaker at these lower frequencies, the calibration of ε_{noise} was done with more precision by measuring induced voltage separately before each data point with the current source outputting at the frequency and applied current of the data point but without a sample. The plateau where χ_{eff} was independent of frequency occurred for $f < 200$ Hz for these cylinders, so the reported χ_{eff} was obtained from a weighted average of data in that range.

Values of χ_{eff} for these particle aspect ratio $\gamma_p = 6.3$ cylinders are shown as a function of packing fraction ϕ in Fig. 13. We only report χ_{eff} for samples shaken in the vortex mixer, as samples shaken vertically to intentionally align particles showed an increase in χ_{eff} of typically 20%, as found in Fig. 12. χ_{eff} increases with ϕ for cylinders as it does for spheres for $\phi < \phi_c$. We do find a decrease in χ_{eff} as ϕ increases above ϕ_c, as expected due to the inability of particles to rearrange for $\phi > \phi_c$. The prediction of Eq. (7) for aspect ratio $\gamma_p = 6.3$ is shown as the solid line in Fig. 13. The prediction is again well above the data, by a factor of 3 or more. A correction for the variation of sample aspect ratio

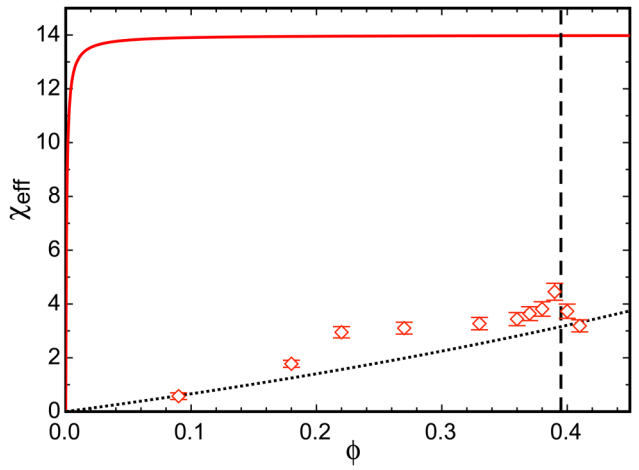

FIG. 13. Effective susceptibility χ_{eff} as a function of packing fraction ϕ for particle aspect ratio $\gamma_p = 6.3$ cylinders. Solid line: model of Eq. (7) for $\gamma_p = 6.3$. Dotted line: model of Eq. (7) for spheres ($\gamma_p = 1$). Vertical dashed line: the packing fraction of the liquid-solid transition. The model still overestimates χ_{eff} by a factor of 3 or more for suspensions of randomly aligned cylinders, regardless of whether they are in a liquid or solid state.

γ_g from the dilution according to Eq. (7) would not increase χ_{eff} by more than 10% for any data point, not nearly enough to match the prediction shown in Fig. 13. The disagreement with prediction confirms that even in the liquid state, the random arrangement and orientation of particles in suspension produces a strong demagnetization effect even for large particle aspect ratios, precluding the larger χ_{eff} predicted by Skomski *et al.*[1]

For comparison to spherical particles, we also plot the prediction of Eq. (7) for aspect ratio 1 as the dotted line in Fig. 13. While the aspect ratio $\gamma_p = 6.3$ particles do not reach the large χ_{eff} predicted by Skomski *et al.*,[1] they at least have a slightly higher χ_{eff} than spheres and reach up to $\chi_{eff} = 4.5$ at the highest packing fraction of the liquid state ($\phi = 0.39$), the largest χ_{eff} we have found of any combination of parameters in suspensions.

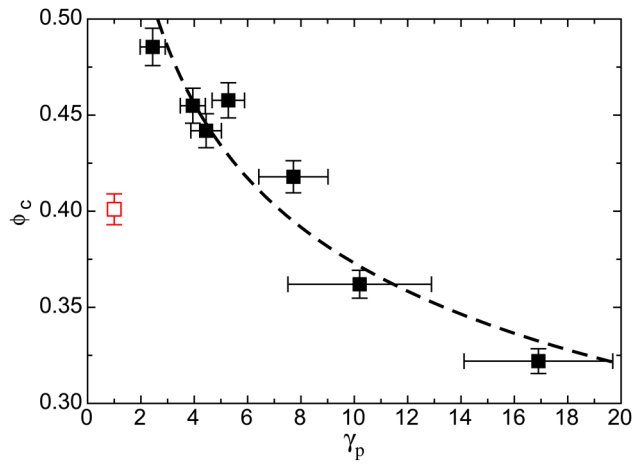

FIG. 14. Packing fraction of the liquid-solid transition ϕ_c as a function of particle aspect ratio γ_p. Solid symbols: suspensions of cylinders. Open symbol: suspension of spheres. Dashed line: power law fit to data for cylinders.

Since these measurements are all performed in static flows, we comment on what level of alignment might be expected in our desired application of turbulent flow. We hypothesize that particle will align with the magnetic field if the field-dipole stress τ_B is the strongest stress acting on the particles. In our measurements, we estimate this to be $\tau_B = \chi_{eff}\mu_0 H_{app}^2/[2(1+\chi_{eff})] = 0.016$ Pa at our maximum field strength and effective susceptibility (where μ_0 is the permeability of a vacuum). In contrast, we estimate the gravitational stress on our cylindrical particles $\Delta\rho g a$ to be between 1.3 Pa and 4.2 Pa for our cylindrical particles (where g is the acceleration of gravity, $\Delta\rho$ is the density difference between particles and liquid, and a is a relevant dimension of the cylinder depending on its orientation), suggesting the cylindrical particles likely settle in our measurements of χ_{eff}. That could explain why the measurements of χ_{eff} do not agree with the model of Eq. (7), as the settling may make it harder for the particles to align better with the applied magnetic field. At the magnetic field strength of the Cadarache dynamo, $\tau_B = 5$ Pa,[4] while we would expect to need a turbulent shear stress of at least $\tau_U = 0.02\rho U^2 = 35$ kPa to achieve such a dynamo with our suspensions (where ρ is the particle density and U is a typical flow velocity).[7] Thus, in the turbulent flow experiments that we would like to use such suspensions, the turbulent shear stress is expected to be dominant and would be expected to cause the particles to follow eddies and arrange randomly as long as the particles are smaller than most of the eddies. This would still be expected to result in lower χ_{eff} than the model prediction, as found in Figs. 13 or 12.

IV. SUMMARY

In this paper, we reported measurements of the effective magnetic susceptibility χ_{eff} of suspensions in the limit of weak applied magnetic fields as a function of packing fraction ϕ, sample aspect ratio γ_g, and particle aspect ratio γ_p. For spherical particles, or for non-spherical particles aligned with the applied magnetic field, we find the model of Skomski *et al.*[1] can be fit with power laws for the demagnetization factors D_g and D_p describing the aspect ratio dependence of the sample and particles, respectively, in the form of Eq. (7) (Figs. 8–10). Over the range $0 \le \phi \le 0.407$ (up to the liquid-solid transition ϕ_c), $2.5 \le \gamma_g \le 32$, and $1 \le \gamma_p \le 20$, the fit was accurate within a root-mean-square difference of 13%. This fit yields $D_g = 0.33\gamma_g^{-1.11}$, consistent with values obtained for single-piece cylindrical solids over a smaller parameter range[12] and $D_p = 0.15\gamma_p^{-4.4}$. The agreement with the model for different particle shapes suggests the model can account for the demagnetization effect for different particle shapes, even though it was originally derived only for ellipsoids. Since the model parameters were self-consistently fit to particles of different shapes (i.e., spheres and cylinders) as well as dry granular materials, then the same model parameters apply for a variety of particle shapes and with or without liquid within the 13% error. Due to its characterization of the demagnetization effect, the model Skomski *et al.* expressed in Eq. (7) with the fit coefficients obtained in Figs. 8–10 more accurately describes $\chi_{eff}(\phi, \gamma_g)$

for suspensions of spherical particles than the model of Martin *et al.*[15]

For non-spherical particles aligned with the magnetic field, the model of Skomski *et al.* successfully predicted that the demagnetization effect would be weaker and the bulk susceptibility could be reached in the limit of large aspect ratio γ_p and sample aspect ratio γ_g.[1] However, this was only found to apply to suspensions if we manually forced the particles to be aligned (Fig. 10). In realistic suspensions of randomly oriented particles, we found $\chi_{eff} \approx 4$ in the limit of large γ_p, and the largest effective susceptibility we found was only $\chi_{eff} = 4.5$, for cylinders of particle aspect ratio $\gamma_p = 6.3$ and sample aspect ratio $\gamma_g = 4.1$ (Fig. 12). This χ_{eff} is only 10% higher than for spheres,[15] indicating only a modest improvement in χ_{eff} when using large aspect ratio particles. The model prediction overestimates the measured χ_{eff} by a factor of 3 or more in the cases we tested (Figs. 12 and 13). This disagreement is the result of the random orientations of particles in dense suspensions (Figs. 11–13), which is not accounted for in the model. The random orientations of particles likely enhance the demagnetization effect. Accounting for the misalignment of particles would lead to a more complete model for χ_{eff}. The dependence of χ_{eff} on the alignment of particles (Figs. 11 and 12) means that χ_{eff} can vary with different packing procedures and in different flow fields for non-spherical particles and is not just a function of ϕ, γ_p, and γ_g. We also observed that $\chi_{eff}(\gamma_p)$ displays a local maximum at $\gamma_p \approx 5$ for $\gamma_g = 4.1$ (Fig. 12). Since it was predicted that the maximum χ_{eff} would increase monotonically with γ_p,[1] this feature was unexpected and remains unexplained.

Since we performed measurements of χ_{eff} in the linear material response limit, it is worth mentioning how these results apply to other regimes. We note that the more exact expressions of Eqs. (1) and (2) should still be used instead of Eq. (3) in cases where χ_{eff} approaches χ. Since we found χ_{eff} no larger than about 4, then the situation where χ_{eff} approaches χ is not likely for good ferromagnetic materials unless much larger χ_{off} are found. On the other hand, for large magnetic field strength when the magnetization becomes saturated, the material susceptibility χ becomes smaller. In such a case, the same demagnetization factors D_p and D_g are still expected to apply at different H, since the former are functions of geometry, while the latter is a material property. For ferromagnetic materials whose linear susceptibility χ is on the order of 10^3, the non-linear susceptibility would not make a dominant contribution to the value of χ_{eff} until applied magnetic fields reach the order of 10^2 to 10^3 times the saturation field strength for values of χ_{eff} on the order of 1 to 10. Such high values of applied magnetic field can still give the same result of the linear response region because the demagnetization effect greatly reduces the local magnetic field inside the particles.

Another prediction based on the model of Martin *et al.*[15] that χ_{eff} would diverge to approach the material susceptibility χ at the packing fraction ϕ_c where particles come into contact also fails dramatically, as we observe only $\chi_{eff} \approx 4$ in the limit of ϕ_c at the liquid-solid transition (Fig. 8). The demagnetization effect again limits χ_{eff} and prevents such a divergence of χ_{eff} at any ϕ for spherical particles, which was not accounted for in the model of Martin *et al.*[15]

The failures to achieve the predicted χ_{eff} approaching χ for large particle aspect ratio γ_p or large packing fraction ϕ may limit applications of magnetic suspensions, as $\chi_{eff} \approx \chi$ would have allowed for much stronger magnetic responses of suspensions, comparable to large-aspect ratio ferromagnetic materials. Rather, these results suggest that suspensions of spherical particles have nearly the χ_{eff} as large aspect ratio rods, and the modest improvement of 20% achieved for a specific aspect ratio of rods may not be worth the added complications of dealing with the added variable of particle alignment in many applications. Nonetheless, there is a significant range of tunable magnetic properties of magnetic suspensions up to $\chi_{eff} \approx 4$, several orders of magnitude stronger than pure paramagnetic fluids, which typically have χ in the range of 10^{-9} to 10^{-4}. The viscosity is also tunable over several decades, and the linearity of the magnetic response without hysteresis, like paramagnetic materials, can also be desirable for simple control.[7]

ACKNOWLEDGMENTS

We thank Ethan Kyzivat for helping out with preliminary experiments. We acknowledge financial support from NSF Grant Nos. CBET-1255541 and AFOSR FA 9550-14-1-0337.

APPENDIX: VALUES OF ϕ_c FOR DIFFERENT PARTICLE ASPECT RATIOS

To compare χ_{eff} for particles of different shape in a meaningful way requires identifying the packing fraction of the liquid-solid transition ϕ_c for each shape. ϕ_c was measured for each particle aspect ratio γ_p by observing the change in surface reflectivity as the particles poked through the liquid-air interface of the suspension when $\phi > \phi_c$. It has been confirmed that this gives the same result as more traditional methods such as measuring a yield stress.[22] This transition is sharp and easily observed, allowing us to measure it with an uncertainty on ϕ_c of ± 0.01. ϕ_c is plotted as a function of particle aspect ratio γ_p in Fig. 14. The horizontal error bars indicate the standard deviation of particle aspect ratios due to the variation in cut particle lengths. The measured ϕ_c decreases with increasing γ_p for cylinders, consistent with previous results.[23] For later input into models, a power law is fit to ϕ_c for cylinders, yielding $\phi_c = 0.62\gamma_p^{-0.22}$. For comparison, we also plot ϕ_c for the spherical particles used in earlier sections in Fig. 14. The value of ϕ_c for the spheres does not follow the same trend as the cylinders, not only because of the particle shape, but also the different material source may subtly affect interparticle interactions that can have a significant effect on ϕ_c.[24]

[1]R. Skomski, G. C. Hadjipanayis, and D. J. Sellmyer, "Effective demagnetizing factors of complicated particle mixtures," IEEE. Trans. Magn. **43**, 2956–2958 (2007).
[2]R. E. Rosensweig, *Ferrohydrodynamics* (Courier Corporation, 2013).
[3]J. de Vicente, D. J. Klingenberg, and R. Hidalgo-Alvarez, "Magnetorheological fluids: a review," Soft Matter **7**, 3701–3710 (2011).
[4]R. Monchaux, M. Berhanu, M. Bourgoin, M. Moulin, P. Odier, J.-F. Pinton, R. Volk, S. Fauve, N. Mordant, F. Pétrélis, A. Chiffaudel, F. Daviaud, B. Dubrulle, C. Gasquet, L. Marié, and F. Ravelet,

"Generation of a magnetic field by dynamo action in a turbulent flow of liquid sodium," Phys. Rev. Lett. **98**, 044502 (2007).
[5]R. Stieglitz, and U. Müller, "Experimental demonstration of a homogeneous two-scale dynamo," Phys. Fluid. **13**, 561–564 (2001).
[6]A. Gailitis, O. Lielausis, S. Dement'ev, E. Platacis, A. Cifersons, G. Gerbeth, T. Gundrum, F. Stefani, M. Christen, H. Hanel, and G. Will, "Detection of a flow induced magnetic field eigenmode in the riga dynamo facility," Phys. Rev. Lett. **84**, 4365–4368 (2000).
[7]F. Carle, K. Bai, J. Casara, K. Vanderlick, and E. Brown, "Development of magnetic liquid metal suspensions for magnetohydrodynamics," Phys. Rev. Fluid. **2**, 013301 (2017).
[8]A. Aharoni, "Demagnetizing factors for rectangular ferromagnetic prisms," J. Appl. Phys. **83**, 3432–3434 (1998).
[9]B. Bleaney and R. A. Hull, "The effective susceptibility of a paramagnetic powder," Proc. R. Soc. Lond. A. Math. Phys. Eng. Sci. **178**, 86–92 (1941).
[10]R. Bjørk, and C. R. H. Bahl, "Demagnetization factor for a powder of randomly packed spherical particles," Appl. Phys. Lett. **103**, 102403 (2013).
[11]M. D. Dickey, R. C. Chiechi, R. J. Larsen, E. A. Weiss, D. A. Weitz, and G. M. Whitesides, "Eutectic Gallium-Indium (EGaIn): a liquid metal alloy for the formation of stable structures in microchannels at room temperature," Adv. Funct. Mater. **18**, 1097–1104 (2008).
[12]D. X. Chen, E. Pardo, and A. Sanchez, "Fluxmetric and magnetometric demagnetizing factors for cylinders," J. Magn. Magn. Mater. **306**, 135–146 (2006).
[13]We use the magnetometric demagnetization factors and logarithmically interpolate between $\chi = 99$ and $\chi = 999$ to obtain values for $\chi = 850$.
[14]Bjork *et al.*[10] reported demagnetization factors D, which we converted to $\chi_{eff} = \phi/D$. Their aspect ratio was defined as the inverse of our aspect ratio definition.
[15]A. Martin, P. Odier, J.-F. Pinton, and S. Fauve, "Magnetic permeability of a diphasic flow, made of liquid gallium and iron beads," Eur. Phys. J. B Condens. Matter Complex Syst. **18**, 337–341 (2000).
[16]P. Frick, S. Khripchenko, S. Denisov, D. Sokoloff, and J.-F. Pinton, "Effective magnetic permeability of a turbulent fluid with macroferroparticles," Eur. Phys. J. B Conden. Matter Complex Syst. **25**, 399–402 (2002).
[17]M. E. Cates, J. P. Wittmer, J.-P. Bouchaud, and P. Claudin, "Jamming, force chains, and fragile matter," Phys. Rev. Lett. **81**, 1841 (1998).
[18]C. O'Hern, S. A. Langer, A. J. Liu, and S. R. Nagel, "Random packings of frictionless particles," Phys. Rev. Lett. **88**, 075507 (2002).
[19]T. S. Majmudar, M. Sperl, S. Luding, and R. P. Behringer, "Jamming transition in granular systems," Phys. Rev. Lett. **98**, 058001 (2007).
[20]K. W. Desmond, and E. R. Weeks, "Random close packing of disks and spheres in confined geometries," Phys. Rev. E **80**, 051305 (2009).
[21]E. Brown, H. Zhang, N. A. Forman, B. W. Maynor, D. E. Betts, J. M. DeSimone, and H. M. Jaeger, "Shear thickening in densely packed suspensions of spheres and rods confined to few layers," J. Rheol. **54**, 1023–1046 (2010).
[22]E. Brown, H. Zhang, N. A. Forman, B. W. Maynor, D. E. Betts, J. M. DeSimone, and H. M. Jaeger, "Shear thickening and jamming in densely packed suspensions of different particle shapes," Phys. Rev. E **84**, 031408 (2011).
[23]A. P. Philipse, "The random contact equation and its implications for (colloidal) rods in packings, suspensions, and anisotropic powders," Langmuir **12**, 1127–1133 (1996).
[24]V. Trappe, V. Prasad, L. Cipelletti, P. N. Segre, and D. A. Weitz, "Jamming phase diagram for attractive particles," Nature **411**, 772–775 (2001).